Chapter 3

Non-resonant type pressure driven instabilities in stellarators

3.1 Introduction

Although Mercier criterion is useful for investigating the pressure driven instabilities in tokamaks [119] and stellarators [118], it does not predict the limiting conditions in some cases within the ideal MHD model [107, 108]. For deriving the Mercier criterion it is assumed that the unstable mode is radially localized near the mode resonant surface. There is a tendency that the radial mode structure becomes narrow in the vicinity of the mode resonant surface with the increase of mode number. Even the interchange mode with $m = 1/n = 1$ also has a property that the radial mode structure becomes highly localized near the marginal regime [126], where m (n) is a poloidal (toroidal) mode number. This result explains why the Mercier limit correlates with the beta limit due to the interchange instabilities with the low mode numbers [104, 67]. However, this situation changes substantially, when the pressure gradient becomes locally flat at the mode resonant surface [144]. Details of pressure profile effect on the interchange modes will be shown in this paper with use of a cylindrical plasma model for a low shear stellarator with a magnetic hill.

In order to destabilize the interchange mode, the resonant surface is not always necessary. It is reasonable that in a low shear region with a steep pressure gradient, non-resonant modes approximately satisfying the resonant condition are destabilized. First unstable non-resonant resistive modes were shown for a Heliotron-E plasma with a highly peaked pressure profile [86]. Recently ideal non-resonant modes were shown unstable in the central region of Heliotron-E [48], which seems consistent with the $m = 2/n = 1$ mode triggering the sawtooth [156]. It is noted that non-resonant modes usually have global mode structures, which requires numerical

analysis to clarify the property. For studying the details of ideal non-resonant instabilities we use a cylindrical plasma model which saves computational time greatly. Since the non-resonant mode is hard to be excited in a high shear region, our interest is in a low shear stellarator with a magnetic hill.

It is noted that Fu *et al.* [67] studied the relation between the Mercier modes and the low-n modes with a full 3-D stability code for $l = 2$ stellarators. They found that the unstable localized low-n modes are correlated with the Mercier criterion. However, the stability of global-type low-n modes was found to be decorrelated from that of Mercier modes for the case with a fairly large outward magnetic axis shift. It seems that the strong poloidal coupling in the toroidal geometry is essential for this type of unstable mode which may be a tokamak-type ballooning mode. In this paper our interest is in the decorrelation between the low-n pressure driven modes and the Suydam modes in the cylindrical model. Thus both the rotational transform and pressure profiles are important here.

In Sec. 3.2, we derive an eigenmode equation for studying linear interchange modes in stellarators, which is derived from the reduced MHD equations [125]. In Sec. 3.3, we first solve the eigenmode equation analytically in the low shear limit, and discuss about the non-resonant mode. Next we solve the same eigenvalue equation numerically for a finite shear case in Sec. 3.4. Here we show examples to highlight various properties for both the resonant and non-resonant modes. Finally in Sec. 3.5, we summarize the obtained results and give some physical interpretations for the behavior of non-resonant mode.

3.2 Eigenmode equation

For analyzing pressure driven instabilities in stellarators, we use the ideal reduced MHD equations which are derived under the specific ordering for stellarators [125]. Intrinsically, stellarator is a three dimensional configuration which is quite difficult and an open problem as a spectral theory. Here, by averaging in toroidal direction, we can reduce the problem into two dimensions which is the same as axially symmetric systems. This approximation is valid for the modes which have toroidally global structures and when the toroidal mode coupling do not play a major role. The equations are written as

$$\partial_t \psi = \boldsymbol{B} \cdot \nabla \phi, \tag{3.1}$$

$$\rho \frac{\mathrm{d}\Delta\phi}{\mathrm{d}t} = -\boldsymbol{B} \cdot \nabla j_z + \nabla\kappa \times \nabla p \cdot \boldsymbol{e}_z, \tag{3.2}$$

$$\frac{\mathrm{d}p}{\mathrm{d}t} = 0, \tag{3.3}$$

where

$$\boldsymbol{B}\cdot\nabla = B_0\partial_z + \nabla\psi\times\boldsymbol{e}_z\cdot\nabla, \tag{3.4}$$

$$\frac{\mathrm{d}}{\mathrm{d}t} = \partial_t + \nabla\phi\times\boldsymbol{e}_z\cdot\nabla, \tag{3.5}$$

$$\kappa = \frac{2r\cos\theta}{R_0} + \frac{\overline{(\nabla\eta)^2}}{B_0^2}, \tag{3.6}$$

$$j_z = -\Delta A_z, \tag{3.7}$$

$$A_z = \psi + \frac{1}{2B_0}\overline{\nabla\langle\eta\rangle\times\nabla\eta}\cdot\boldsymbol{e}_z. \tag{3.8}$$

Here ψ, ϕ, κ', and η denote the poloidal flux function, the stream function, the averaged curvature of the helical magnetic field, and the magnetic field potential due to helical coils, respectively. Bars denote the averaged equilibrium quantities over a single helical period. The quasi-toroidal coordinates are introduced here whose metrics are written as

$$\mathrm{d}\ell^2 = \mathrm{d}r^2 + r^2\,\mathrm{d}\theta^2 + (R_0 + r\cos\theta)^2\,\mathrm{d}\zeta^2, \tag{3.9}$$

where R_0 denotes the major radius of the torus, r the minor radius, θ and $\zeta = z/R_0$ the poloidal and toroidal angle, respectively. Here the perfectly conducting wall is placed at the plasma boundary, and the boundary conditions are given by $B_r = \partial_\theta\psi = 0$, $v_r = \partial_\theta\phi = 0$, and $p = 0$ at $r = a$.

In the following study, we neglect the toroidal effect in the reduced MHD equations. We also assume that the equilibrium quantities do not depend on the poloidal angle θ. This assumption means that the averaged flux surfaces have circular cross section in the large aspect ratio limit. Then the rotational transform is written as

$$\iota(r) \equiv \frac{R_0}{rB_0}\frac{\mathrm{d}\psi_0}{\mathrm{d}r}, \tag{3.10}$$

where the equilibrium poloidal flux function is given by $\psi_0(r)$. Since the correction due to the diamagnetic current gives higher order contribution in this formulation, the rotational transform includes only the vacuum helical field contribution in this approximation.

For the stability analysis, we use the following normalization for variables,

$$\begin{aligned}
&\psi \to aB_0\psi, && \phi \to \frac{aR_0}{\tau_\mathrm{A}}\phi, && t \to \tau_\mathrm{A}t,\\
&p \to p_0(r=0)p, && r \to ar, && j_z \to \frac{B_0}{\mu_0 a}j_z,\\
&\Delta\phi \to \frac{R_0}{a\tau_\mathrm{A}}\Delta\phi, && A_z \to aB_0A_z,
\end{aligned} \tag{3.11}$$

where $\tau_{\rm A} = R_0\sqrt{\mu_0\rho}/B_0$ denotes the poloidal Alfvén time, a the minor radius of the plasma column, respectively. Then the linearized reduced MHD equations can be written as

$$\gamma(\Delta\phi) = -\frac{n-m\iota}{\gamma}\Delta[(n-m\iota)\,\phi] - \frac{D_{\rm s}}{\gamma}\frac{m^2}{r^2}\phi, \tag{3.12}$$

where $D_{\rm s}$ and the averaged helical curvature κ' are expressed as

$$D_{\rm s} = -\frac{\beta_0}{2\epsilon^2}p'\kappa', \tag{3.13}$$

$$\kappa = \epsilon^2 N\Big(r^2\iota + 2\int r\iota\,{\rm d}r\Big). \tag{3.14}$$

Here $\epsilon \equiv a/R_0$ denotes the inverse aspect ratio, $\beta_0 \equiv 2\mu_0 p_0(r=0)/B_0^2$ the central plasma beta value, and N the toroidal period number of the helical field, respectively. In order to derive Eq. (3.12), all perturbed quantities are assumed to be proportional to $\exp[\gamma t - {\rm i}(m\theta + n\zeta)]$, where m (n) denotes the poloidal (toroidal) mode number. In Eq. (3.13), the prime denotes the derivative with respect to the normalized minor radius r. The perpendicular Laplacian operator in Eq. (3.12) is shown as

$$\Delta = \frac{1}{r}\frac{\rm d}{{\rm d}r}\Big(r\frac{\rm d}{{\rm d}r}\Big) - \frac{m^2}{r^2}. \tag{3.15}$$

Then the ordinary differential equation (3.12) for the stream function ϕ with the mode number (m,n) is written as

$$\begin{aligned}
&\frac{{\rm d}^2\phi}{{\rm d}r^2} + \Big[\frac{1}{r} - \frac{2m\iota'(n-m\iota)}{\gamma^2+(n-m\iota)^2}\Big]\frac{{\rm d}\phi}{{\rm d}r} \\
&- \Big\{\frac{m^2}{r^2} + \frac{1}{\gamma^2+(n-m\iota)^2} \\
&\quad\times\Big[\Big(\frac{m\iota'}{r} + m\iota''\Big)(n-m\iota) - \frac{D_{\rm s}m^2}{r^2}\Big]\Big\}\phi = 0,
\end{aligned} \tag{3.16}$$

which is an eigenmode equation with the eigenvalue γ^2.

For solving Eq. (3.16), the boundary condition at the plasma surface $r = 1$ is $\phi = 0$ under the fixed boundary condition. We also impose the regularity of the solution at $r = 0$. With these boundary conditions, we can set up an eigenvalue problem for the eigenvalue or growth rate γ^2 and the corresponding eigenfunction ϕ.

3.3 Analytic solution of eigenmode equation

3.3.1 Eigenmode properties for shearless case

In this subsection, we assume $\iota' = 0$ for obtaining an analytic solution, then Eq. (3.16) is written as

$$\frac{\mathrm{d}^2\phi}{\mathrm{d}r^2} + \frac{1}{r}\frac{\mathrm{d}\phi}{\mathrm{d}r} + \frac{m^2}{r^2}\Big[\frac{D_\mathrm{s}}{\gamma^2 + (n - m\iota)^2} - 1\Big]\phi = 0. \tag{3.17}$$

For the parabolic pressure profile, $p = p_0(1 - r^2)$, the analytic solution is readily obtained with the transformation $\tilde{r} \equiv \{\widetilde{D}_\mathrm{s} m^2/[\gamma^2 + (n - m\iota)^2]\}^{1/2} r$, where $\widetilde{D}_\mathrm{s} = 4\beta_0 N\iota$. From the solution $u \propto J_m(\tilde{r})$ for the (m, n) mode and the boundary condition $u = 0$ at $r = 1$, the growth rate is written as

$$\gamma^2 = \frac{\widetilde{D}_\mathrm{s} m^2}{Z^2(m, k)} - (n - m\iota)^2, \tag{3.18}$$

where $Z(m, k)$ is the k-th zero point of the m-th order Bessel function of the first kind $J_m(\tilde{r})$.

Although the resonant surface does not exist inside the plasma column, it is seen that the mode satisfying $n \simeq m\iota$ is most unstable and the unstable mode has a global structure without localizing in the radial direction unlike the resonant mode. Further we notice that, when there is no magnetic shear, the radial mode structure, $J_m(Z(m, k)r)$, is not affected by the beta value. We notice from Eq. (3.18) that the more unstable mode has the less node number, and the eigenvalue is discrete with respect to k for the specified (m, n). The generalization of this property will be discussed in the next subsection.

Since the left hand side of Eq. (3.18) is proportional to γ^2 and the right hand side is linear with respect to the plasma beta, the relation (3.18) gives a parabolic line in the (β, γ) plane. Thus a small variation in β_0 from the marginal equilibrium may cause an abrupt increase of growth.

The beta limit for stability is obtained by substituting $\gamma^2 = 0$ into Eq. (3.18), which yields

$$\beta_{0\mathrm{c}} = \frac{Z^2(m, k)(n - m\iota)}{4N\iota m^2}. \tag{3.19}$$

In order to examine the beta limit of the higher harmonic modes with same helicity, we use the transformation of the variables $(m, n) \mapsto l(m, n)$, which yields

$$\beta^l_{0\mathrm{c}} = \frac{Z^2(lm, k)(n - m\iota)}{4N\iota m^2}. \tag{3.20}$$

Since $Z(lm, k) > Z(m, k)$ for $l \geq 2$, the beta limit of the higher harmonic mode, $\beta^l_{0\mathrm{c}}$, is higher than the $l = 1$ case, $\beta_{0\mathrm{c}}$. This is different from the resonant modes with the same helicity, which give the same beta limit given by the Suydam criterion [126].

3.3.2 Radial structure of most unstable mode

In this subsection we show that the more unstable mode has the less node number in radial direction with the specified (m, n). We follow the proof shown by Goedbloed and Sakanaka [72, 10]. By introducing a variable $\xi = \phi/r$, the eigenmode equation (3.16) is written in the Sturmian form as

$$\frac{\mathrm{d}}{\mathrm{d}r}\Big(K\frac{\mathrm{d}\xi}{\mathrm{d}r}\Big) - G\xi = 0, \tag{3.21}$$

where

$$K(\gamma^2; r) = r^3[\gamma^2 + (n - m\iota)^2],$$
$$G(\gamma^2; r) = r\{(m^2 - 1)[\gamma^2 + (n - m\iota)^2] + (3m\iota' r + m\iota'' r^2)(n - m\iota) - D_{\mathrm{s}} m^2\}.$$

Let two solutions corresponding to two neighboring growth rates, $\gamma^2 = \gamma_1^2$ and $\gamma_1^2 + \delta\gamma^2$ be ξ_1 and $\xi_1 + \delta\xi$, respectively, which only satisfy the boundary condition at $r = 0$. When we substitute the first solution ξ_1 corresponding to the parameter γ_1^2 in Eq. (3.21), we obtain

$$\frac{\mathrm{d}}{\mathrm{d}r}\Big(K(\gamma_1^2; r)\frac{\mathrm{d}\xi_1}{\mathrm{d}r}\Big) - G(\gamma_1^2; r)\xi_1 = 0. \tag{3.22}$$

Substituting the second solution into Eq. (3.21) and subtracting Eq. (3.22) leads to

$$\frac{\mathrm{d}}{\mathrm{d}r}\Big(K(\gamma_1^2; r)\frac{\mathrm{d}\delta\xi}{\mathrm{d}r}\Big) - G(\gamma_1^2; r)\delta\xi = -\delta\gamma^2\Big[\frac{\mathrm{d}}{\mathrm{d}r}\Big(\frac{\partial K}{\partial\gamma^2}\Big|_{\gamma_1^2}\frac{\mathrm{d}\xi_1}{\mathrm{d}r}\Big) - \frac{\partial G}{\partial\gamma^2}\Big|_{\gamma_1^2}\xi_1\Big]. \tag{3.23}$$

Assume now that $\xi_1(r_1) = 0$ at $0 < r_1 \leq 1$, which is possible for an unstable case. We make the product of $\delta\xi$ with Eq. (3.22), ξ_1 with Eq. (3.23) and integrate from 0 to r_1. Subtracting both sides leads to

$$K\delta\xi\frac{\mathrm{d}\xi_1}{\mathrm{d}r}\Big|_{r_1} = -\delta\gamma^2\int_0^{r_1}\Big[\frac{\partial K}{\partial\gamma^2}\Big(\frac{\mathrm{d}\xi_1}{\mathrm{d}r}\Big)^2 + \frac{\partial G}{\partial\gamma^2}\xi_1^2\Big]\,\mathrm{d}r, \tag{3.24}$$

after some partial integrations, where we have used the fact that $\delta\xi(0) = 0$, $K(\gamma_1^2; 0) = 0$. Here K, G and their derivatives with respect to γ^2 are all evaluated at $\gamma^2 = \gamma_1^2$. Since $\partial K/\partial\gamma^2 = r^3$ and $\partial G/\partial\gamma^2 = r(m^2 - 1)$, the integrand is positive for $m \geq 1$ at all radial points. Provided that $\delta\gamma^2 > 0$, or $\xi_1 + \delta\xi$ is more unstable than ξ_1, the right hand side of Eq. (3.24) becomes negative. Since K is positive in $(0, 1)$, the radial position of $\xi_1 + \delta\xi = 0$ moves to outer due to the increase of the parameter γ^2. Since K and G are monotonic functions of γ^2 for $m \geq 1$, we can conclude that the radial positions of all zeros move to the outer direction with the increase of the parameter γ^2. If we further impose another boundary condition at $r = 1$, it is confirmed that the eigenvalue is discrete and the more unstable mode has the less node number. In other words, the most unstable mode has no node.

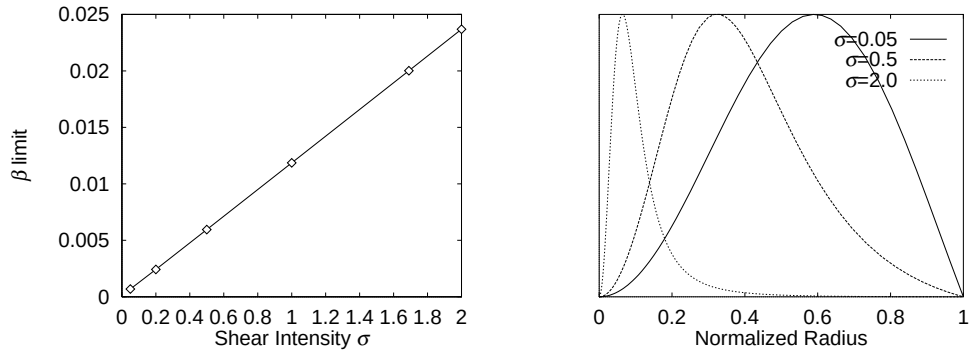

(a) (b)

Figure 3.1: (a) Dependence of the beta limit on the magnetic shear parameter σ for the non-resonant $(2, 1)$ mode. (b) Radial mode structures in cases of $\sigma = 0.05$, 0.5, and 2.0 for the parabolic pressure profile with $\beta_0 = 0.03$.

3.4 Numerical solution of eigenmode equation

3.4.1 Resonant and non-resonant modes for standard pressure profiles

We have solved Eq. (3.16) numerically by the shooting method using the fourth order Runge-Kutta formula. At first we picked up the same eigenvalue problem as shown in section 3.3 in order to validate the numerical code. The obtained growth rates for the $(m, n) = (2, 1)$ mode coincide well with the analytic solution, Eq. (3.18), and the radial mode structures described by the Bessel function $J_2(\tilde{r})$ seems to be unchanged by the variation of β_0.

Next we have investigated the effect of the magnetic shear on the non-resonant modes for the standard parabolic pressure profile. For the assumed rotational transform profile, $\iota = 0.51 + \sigma r^2$, σ is changed from 0.05 to 2.0. The rotational transform profile in the case of $\sigma = 1.69$ is approximately coincides with that in Heliotron-E [48]. When the beta value is fixed, the growth rate of the non-resonant $(2, 1)$ mode is decreased with the increase of the magnetic shear intensity σ. Or the beta limit is increased almost linearly with the increase of σ as shown in Fig. 3.1. The radial mode structure is shifted to the inner region when σ is increased (see Fig. 3.1). This result can be interpreted in the following way. As σ is increased, there are two effects. First, the magnetic shear becomes larger in the outer region compared to the inner region. Second, the outer region is removed further away from the resonance than the inner region. These may account for the mode structure becoming more lo-

calized towards the magnetic axis. Also when β_0 is decreased, since the destabilizing effect due to the plasma pressure gradient becomes weak, the non-resonant mode can be excited only in the inner region. However, since there is no resonant surface, the radial mode structure is not highly localized and still has a global structure. The behavior of the growth rate near the marginal beta value for the non-resonant mode is different from that for the resonant mode as shown in Fig. 3.2. The growth rate of non-resonant mode decreases to zero without the tail at $\beta_0 \simeq \beta_{0c}$, where β_{0c} is the beta limit for the non-resonant $(2,1)$ mode.

Here we study transition from the resonant mode to the non-resonant one. For currentless plasmas in Heliotron-E, MHD equilibria show that the central rotational transform is increased with the increase of beta value. When the vacuum rotational transform at the plasma center is lower than 0.5, the resonant surface for the $(2,1)$ mode exists inside the plasma column. The resonant mode may not be excited due to the low beta value at the initial state. Experimental results show that the $(2,1)$ mode becomes unstable for $\beta_0 \gtrsim 0.7\%$ in the neutral beam heating plasmas, which leads to the occurrence of sawtooth [48]. However, when the ECRH is applied to the central region, the pressure profile becomes more peaked and the $(2,1)$ mode is stabilized. These data could be understood with disappearance of the $\iota = 0.5$ surface according to the increase of the central beta value. Linear stability of the ideal $(2,1)$ mode in the toroidal geometry shows that the resonant mode appears first, then it changes to the non-resonant mode with the increase of β_0. Finally the non-resonant mode becomes stable, when $\iota(0)$ is deviated far from 0.5 [48].

In the cylindrical model we simulate the above situation by changing the central value of the rotational transform artificially. For clarifying the property of the non-resonant mode, we consider a weak shear configuration with the resonant surface for the $(2,1)$ mode at first. Then we exclude the resonant surface of $\iota = 0.5$ by increasing $\iota(0)$. Figure 3.2 shows the numerical results for the pressure profile $p = p_0(1 - r^4)$. White squares correspond to the growth rates for the equilibria with rotational transform profile, $\iota = 0.499 + 0.2r^2$, which has the resonant surface for the $(2,1)$ mode at the normalized radius $r \simeq 0.07$. Black squares correspond to the growth rates for the equilibria with $\iota = 0.501 + 0.2r^2$, which has no resonant surface for the $(2,1)$ mode. The beta limit for the resonant case seems to be 1.14×10^{-3} or less, while for the non-resonant mode it is 5.97×10^{-3}. The difference between these beta limits correlates with the radial mode structure. In the small growth rate regime, when β_0 is decreased, the radial mode structure of the resonant mode becomes more localized. Thus the highly localized mode with an extremely small growth rate is possible as shown in Fig. 3.2. Thus, in the β-γ space the line for the resonant mode case extends to the lower beta region with small growth rates. On the contrary,

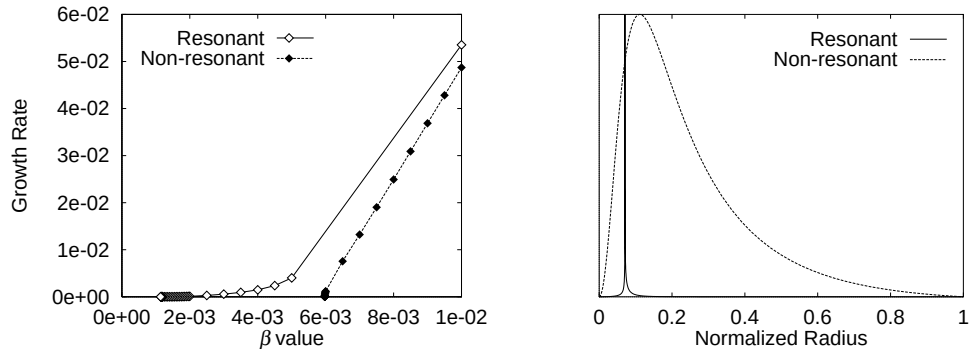

(a) (b)

Figure 3.2: (a) Dependence of the growth rate of $(2,1)$ mode on the central beta value β_0 for $p = p_0(1-r^4)$. Squares denote numerical results. The white ones correspond to the resonant case and the black ones to the non-resonant case. (b) Radial mode structures corresponding to the resonant ($\beta_0 = 1.35 \times 10^{-3}$), and non-resonant case ($\beta_0 = 5.97 \times 10^{-3}$). Here the rotational transform profile is $\iota(r) = 0.499 + 0.2r^2$ for the resonant case and $\iota(r) = 0.501 + 0.2r^2$ for the non-resonant case.

since the non-resonant mode cannot be localized at a particular surface, the growth rate decreases to zero without the tail with the decrease of β_0.

We may apply the Suydam criterion to resonant modes, which can be derived from the indicial equation of Eq. (3.16) at the singular point, or the resonant surface. It is written as

$$\frac{D_{\rm s}}{\iota'^2 r_{\rm s}^2} < \frac{1}{4}, \tag{3.25}$$

for the stability, where $D_{\rm s}$ and ι' are evaluated at the resonant surface, $r = r_{\rm s}$, for the corresponding mode. In the case of Fig. 3.2, the resonant surface of the $(2,1)$ mode is $r_{\rm s} \simeq 0.07$. Here the beta limit obtained from the criterion (3.25) is $\beta_0 \simeq 1.05 \times 10^{-3}$. Generally it is difficult to obtain the beta limit for the resonant mode numerically. One reason is the extension of the growth rate to the low beta side as mentioned above, and the other is the localization of the mode structure in the vicinity of the resonant surface. In Fig. 3.2, however, the difference between the analytic evaluation and the numerical result is less than 10%, and the growth rate at numerically obtained beta limit is 4.49×10^{-11}, which is normalized by poloidal Alfvén time.

It is noted that the global-type mode is shown in Ref. [67] in toroidal stellarators. However, this mode is different from the non-resonant mode shown here, since the poloidal coupling in the toroidal geometry is essential to destabilize the global-type mode.

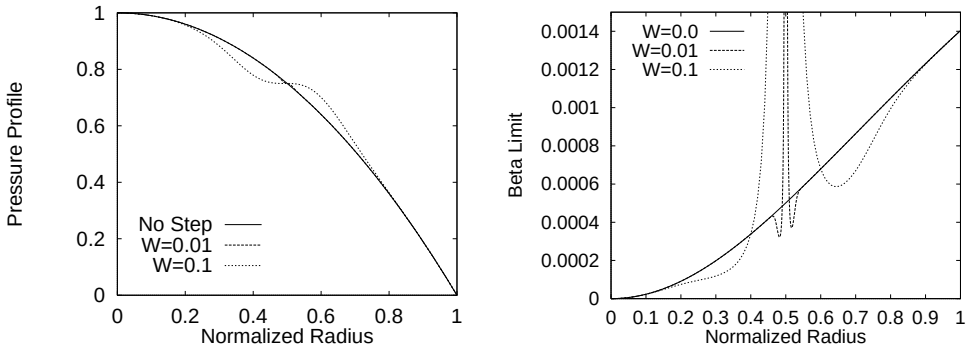

Figure 3.3: Left figure shows the pressure profiles given by Eq. (3.26) for $\lambda = 1$. The effect of pressure flattening is very small for $W = 0.01$. Right figure shows the Suydam critical β corresponding to each W.

3.4.2 Resonant modes for locally flattened pressure profiles at resonant surface

Here we consider equilibria with the resonant surface at $\iota = 0.5$ for the $(2, 1)$ mode in the plasma column, but without the pressure gradient on the resonant surface. In the experimental situation of Heliotron-E there may exist small magnetic islands due to resistive interchange instabilities at the low order resonant surfaces [68, 105], which may be nonlinearly saturated at low fluctuation levels. In such a case the equilibrium may not be violated by the resistive mode, however, the local plasma profile will change and the pressure gradient becomes small near the resonant surface [48, 106]. For this situation the Suydam criterion (3.25) predicts stability at the $\iota = 0.5$ surface.

Here we will show that low m modes can be unstable due to the finite negative pressure gradient at elsewhere other than the resonant surface. For simplicity the pressure profile is assumed as

$$p = 1 - r^2 + \lambda(r - r_{\rm s}) \exp\Big[-\frac{1}{2}\Big(\frac{r - r_{\rm s}}{W}\Big)^2\Big], \tag{3.26}$$

where $r_{\rm s}$ is the position of the mode resonant surface, and the choice $\lambda = 2r_{\rm s}$ makes p' vanish at $r = r_{\rm s}$. The width of the flat region is controlled with the parameter W. Several pressure profiles given by Eq. (3.26) and corresponding critical β_0 values evaluated by Suydam criterion (3.25) are shown in Fig. 3.3. We assume $\iota = 0.45 + 0.2r^2$ and consider the $(2, 1)$ mode again. The resonant surface exists at $r_{\rm s} = 0.5$ where the pressure gradient vanishes. We can see that the pressure flattening region is very narrow in $W = 0.01$ case, which connects with the steepness of the pressure gradient near resonant surface, therefore, the destabilizing effect around resonant surface is considerably large. However, we consider that the high

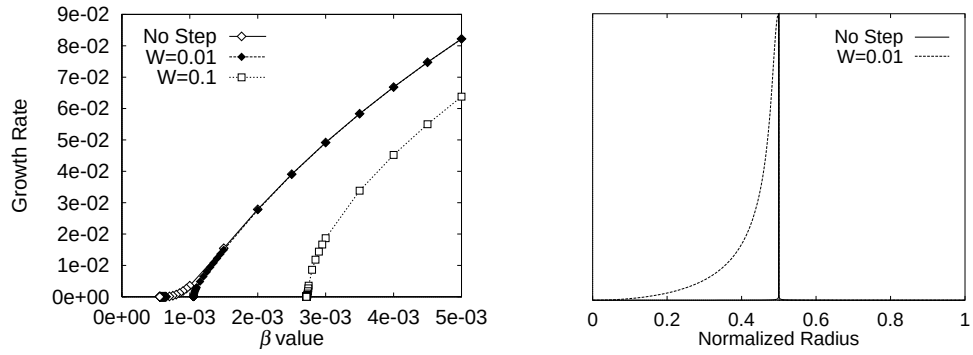

(a) (b)

Figure 3.4: (a) Dependence of the growth rate of $(2,1)$ mode on the central beta value β_0 for $W = 0$, 0.01 and 0.1. (b) Radial mode structures for $W = 0$ ($\beta_0 = 5.62\times10^{-4}$), and $W = 0.01$ ($\beta_0 = 1.05 \times 10^{-3}$). The radial mode structures for $W = 0.1$ are shown in Fig. 3.5.

(m, n) modes which has resonant surface close to $\iota \simeq 0.5$ might be stabilized by non-MHD effect.

For three cases with $W = 0$, 0.01, and 0.1 shown in Fig. 3.3, growth rates of the $(2, 1)$ mode are shown as a function of β_0 in Fig. 3.4(a). Although the highly localized mode structure is observed in the case of $W = 0$, it is not localized even in the case of $W = 0.01$, and the beta limit is increased with a factor of 2. Furthermore, in Fig. 3.4(a) the growth rate decreases to zero without the tail near the beta limit for $W = 0.01$, while the growth rate in the higher beta regime is not affected. The growth rates and the radial mode structures in the case of $W = 0.1$ are shown separately in Fig. 3.5, where both the first growing mode with the maximum growth rate and the second growing mode with the next growth rate are shown. In Figs. 3.4(b) and 3.5(b) we see that the radial mode structures are quite different from the case with $W = 0$. They are restricted in one side of the mode resonant surface, and change sharply at the mode resonant surface in the case of $W \neq 0$. In order to understand the role of the second growing mode, it is interesting to study nonlinear behavior of the $(2, 1)$ mode for an equilibrium with a flat pressure region in the neighborhood of resonant surface. It is considered that, since the average magnetic shear is weak in the inner side of the resonant surface, the first growing mode is restricted to the region $[0, r_s]$ in the case of $W = 0.01$, whereas in the case of $W = 0.1$, it is restricted to the outer region since the average pressure gradient seems larger in the outer side. It is noted that the beta limit of the $W = 0.01$ case, $\beta_{0c} = 1.0 \times 10^{-3}$, is lower than that of the $W = 0.1$ case, $\beta_{0c} = 2.7 \times 10^{-3}$. In both

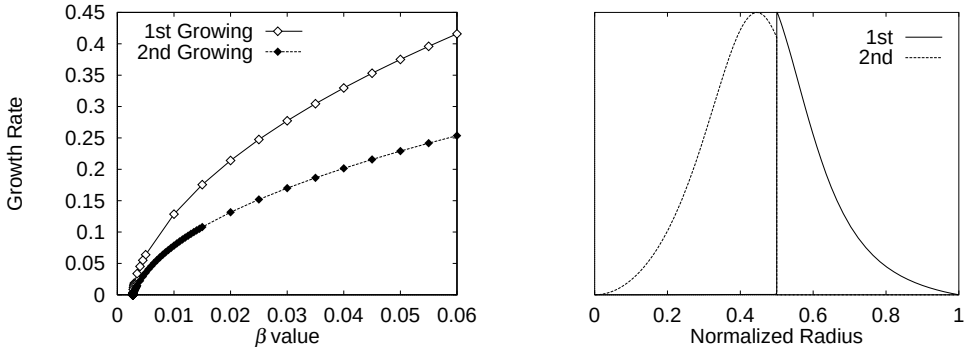

(a) (b)

Figure 3.5: (a) Dependence of the growth rate of $(2,1)$ mode on the central beta value β_0 for $W = 0.1$. (b) Radial mode structure of the first growing mode ($\beta_0 = 2.72 \times 10^{-3}$) and that of the second growing mode ($\beta_0 = 2.76 \times 10^{-3}$). It is noted that the growth rates of the first growing mode are the same as those in Fig. 3.4(a).

cases the second growing mode appears in the opposite region to the first growing mode.

To investigate why the steep mode structure appears at the resonant surface, we expand the coefficients in Eq. (3.16) in the neighborhood of the mode resonant surface $r = r_{\rm s}$. Since the rotational transform is expanded as $\iota(r) \approx \iota(r_{\rm s}) + \iota'(r_{\rm s})(r - r_{\rm s}) + \cdots$, the resonant denominator is expressed as

$$n - m\iota \approx -m\iota'(r_{\rm s})(r - r_{\rm s}) + \cdots. \tag{3.27}$$

Since the pressure becomes flat at the mode resonant surface, $p'(r_{\rm s})$ becomes zero, but $p'(r)$ is still negative in both sides of the mode resonant surface. Therefore p'' is also zero at $r = r_{\rm s}$, thus p' is expanded in the neighborhood of the mode resonant surface as

$$p' \approx \frac{p'''(r_{\rm s})}{2}(r - r_{\rm s})^2 + \cdots, \tag{3.28}$$

where $p'''(r_{\rm s}) < 0$. Substituting the leading terms of Eqs. (3.27) and (3.28) into Eq. (3.16) yields

$$\begin{aligned} &\frac{{\rm d}^2\phi}{{\rm d}r^2} + \Big[\frac{1}{r} + \frac{2m^2\iota'^2(r - r_{\rm s})}{\gamma^2 + m^2\iota'^2(r - r_{\rm s})^2}\Big]\frac{{\rm d}\phi}{{\rm d}r} \\ &- \Big[\frac{m^2}{r^2} - \frac{m\iota'(r - r_{\rm s})}{\gamma^2 + m^2\iota'^2(r - r_{\rm s})^2}\Big(\frac{m\iota'}{r} + m\iota''\Big) \\ &\quad + \frac{m^2\beta_0 N p'''(4r_{\rm s}\iota + r_{\rm s}^2\iota')}{4r_{\rm s}^2[\gamma^2 + m^2\iota'^2(r - r_{\rm s})^2]}(r - r_{\rm s})^2\Big]\phi = 0. \end{aligned} \tag{3.29}$$

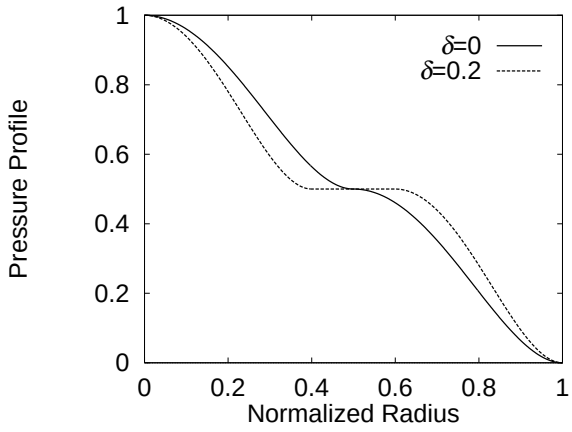

Figure 3.6: Pressure profiles with the locally flat regions around the mode resonant surface. The solid line corresponds to Eq. (3.30) and the broken line to Eq. (3.31).

As seen here, the effect of the pressure near the resonant surface appears in the higher order with respect to $(r - r_s)$. Thus the pressure is negligible and does not affect the steep mode structure.

In order to confirm this situation, we have calculated the radial mode structure of nearly marginal mode for the following pressure profiles numerically. One is

$$p = \begin{cases} \dfrac{1}{2}(1-4r^2)^2 + 0.5 & (r < 0.5), \\ \dfrac{1}{2}[1-4(r-0.5)^2]^2 & (r > 0.5), \end{cases} \tag{3.30}$$

and the other is

$$p = \begin{cases} \dfrac{1}{2}\left(1 - \dfrac{25}{4}r^2\right)^2 + 0.5 & (r < 0.4), \\ 0.5 & (0.4 < r < 0.6), \\ \dfrac{1}{2}\left[1 - \dfrac{25}{4}(r-0.5)^2\right]^2 & (r > 0.6). \end{cases} \tag{3.31}$$

The latter pressure profile contains a completely flat region whose width is noted as δ in $[0.4, 0.6]$ in order to eliminate the effect of the pressure gradient. Those profiles are shown in Fig. 3.6. By assuming the same rotational transform profile as the previous case in Figs. 3.4 and 3.5, the obtained mode structures are shown in Fig. 3.7. The reason why the mode structure of the first growing mode is restricted in the inner region is that, since the average pressure gradient is equal in both sides of $r = 0.5$, the interchange mode is considered to be excited in the weaker shear region. It is interesting that the mode structure with the sharp decrease at $r = r_s$ is observed even though the pressure is completely flat in a region with a finite width

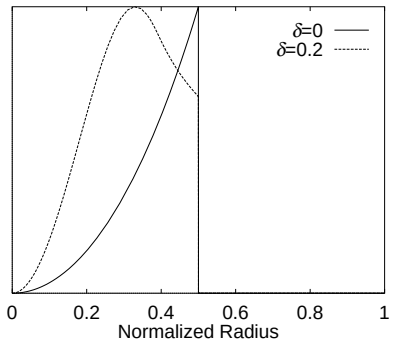

(a)

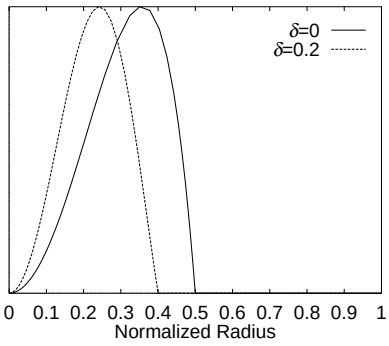

(b)

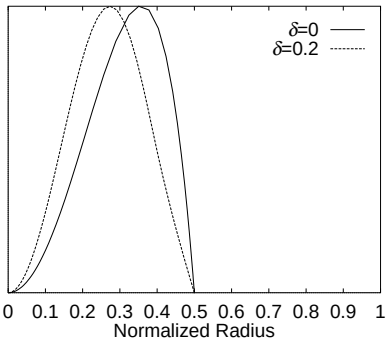

(c)

Figure 3.7: (a) Radial mode structures of $(2, 1)$ mode for the pressure profile corresponding to Eq. (3.30) ($\delta = 0$ curves) and to Eq. (3.31) ($\delta = 0.2$ curves). Both lines show the radial mode structure of each first growing mode. Here all perturbed functions are shown; (a) $\tilde{\phi}$, (b) $\tilde{p}$, (c) $\tilde{\psi}$.

around the mode resonant surface. This assures our conjecture that the locally steep profile of the mode structure such as in Figs. 3.5 and 3.7 is caused only by the profile of the magnetic shear, not by the pressure profile any more. We note that a *non-resonant feature* is seen in the radial mode structure for the second growing mode in Fig. 3.5(b) and the first growing mode for the second pressure profile (3.31) in Fig. 3.7(b), i.e. the peak is shifted from the resonant surface. This clearly shows that the unstable mode is driven by the negative pressure gradient at elsewhere other than the resonant surface.

The appearance of the sharp decrease to zero at the resonant surface in the radial mode structure or $u(r)$ is considered as follows. Consider a resonant layer satisfying $|r - r_{\rm s}| = |x| \sim \epsilon$. Since our interest is in the small growth rate limit, $\gamma \sim \epsilon$ is also assumed. Under these assumptions, if we assume $p' \simeq 0$ in the resonant layer, the

second term in Eq. (3.21) becomes negligible and

$$\frac{\mathrm{d}}{\mathrm{d}r}\Big(K(\gamma^2;r)\frac{\mathrm{d}\xi}{\mathrm{d}r}\Big) = 0 \tag{3.32}$$

decide the behavior of eigenfunction $\xi(r)$ in the resonant layer. It is noted that Eq. (3.32) is exactly same as that given by Rosenbluth, Dagazian and Rutherford for the $m = 1$ internal kink mode in the cylindrical tokamak [113]. They gave the solution

$$\xi = \frac{1}{2}\xi_a\Big[1 - \frac{2}{\pi}\arctan\Big(\Big|\frac{m\iota'}{\gamma}\Big|x\Big)\Big], \tag{3.33}$$

for the boundary conditions $\xi \to \xi_a$ as $x \to -\infty$ and $\xi \to 0$ as $x \to \infty$. Since $m\iota'/\gamma \sim O(\epsilon^{-1})$, the eigenfunction ξ has the largest gradient at $r = r_\mathrm{s}$ and has a step function structure near the resonant surface. Further, since $u \simeq r_\mathrm{s}\xi$ in the neighborhood of the resonant layer, this type of solution may explain the behavior of the sharp decrease to zero of the eigenfunction with the largest growth rate near the resonant surface $r = r_\mathrm{s}$ for $\gamma \to 0$.

3.4.3 Behavior of non-resonant type mode

We will show that the non-resonant type mode is also excited even if pressure profiles do not have exact zero gradient at the resonant surface. For small and nonzero values of p' at $r = r_\mathrm{s}$, we discuss about transition from the resonant mode to the non-resonant type one. We assume $p = p_0(1 - r^2)^\alpha$, where α is changed from 4 to 14 (see Fig. 3.8). The profile of the rotational transform is fixed as $\iota = 0.4 + 0.2r^2$, where the resonant surface for the $(2, 1)$ mode exists at $r_\mathrm{s} = \sqrt{2}/2$. Figure 3.8 shows that the mode structure gradually changes from the resonant one to the non-resonant type one. Particularly the $\alpha = 14$ case shows that the peak of the radial mode structure exists at the position different from the resonant surface, which is considered as the non-resonant feature. It does have a step function structure instead of a peak at the mode resonant surface for the nearly marginal beta value. In other words, the driving force to the instability comes from the largest pressure gradient region different from the resonant surface. From the sharp decrease of ϕ to zero at the resonant surface in the $\alpha = 14$ case, it is considered that the pressure has almost no effect on the mode structure at the resonant surface, since p' and p'' are negligibly small. In the $\alpha = 10$ case, the mode structure has the maximum value at the resonant surface; however, there exists another broad peak in the inner side of the resonant surface. Also the growth rate vanishes without the tail near the beta limit (see Fig. 3.8(b)). In the $\alpha = 8$ case, the situation is more ambiguous. The mode structure has a maximum value at the resonant surface and has no other peak. However, the dependence of γ on β near the beta limit is different from the standard

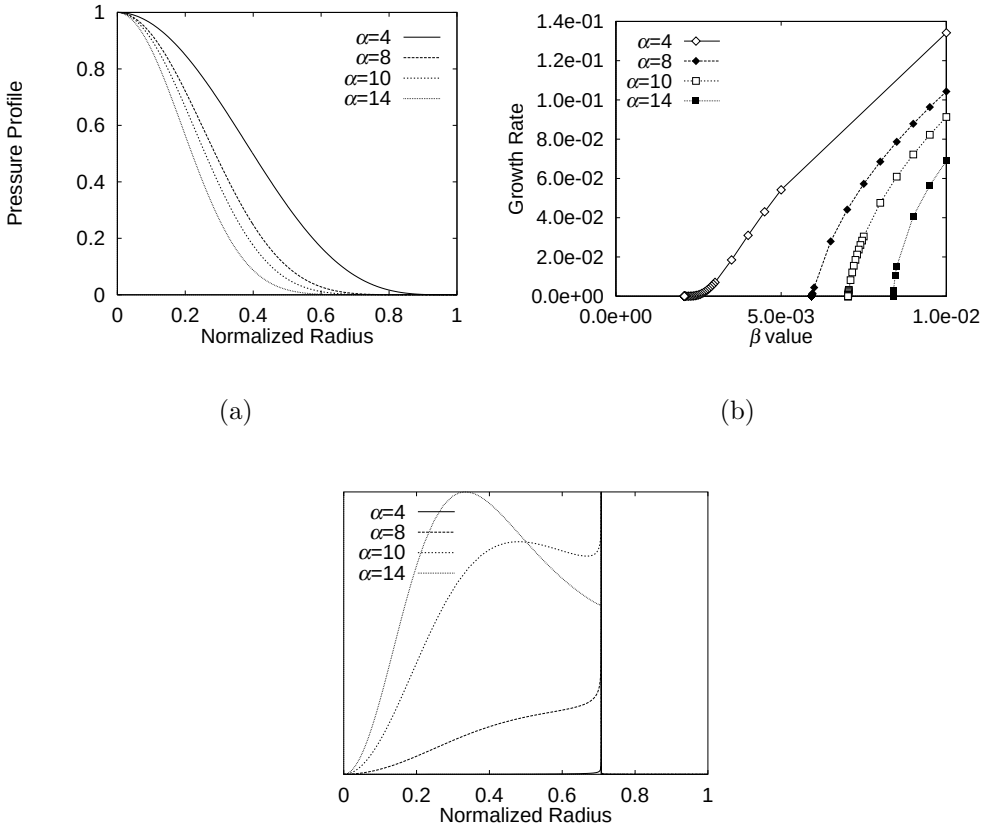

Figure 3.8: (a) Pressure profiles given by $p = p_0(1 - r^2)^\alpha$ for $\alpha = 4$, 8, 10, and 14. (b) Dependence of the growth rate on the central beta value β_0 for different α. (c) Radial mode structures near the beta limit for different α. The height of the mode structure is normalized with its own maximum value.

resonant mode. Thus the case with $\alpha = 8$ or 10 seems to have a mixed property between the resonant and non-resonant type mode. For the $\alpha = 4$ case, the clear feature of the resonant mode is seen, i.e. the small growth rate regime is extended to the low beta side in the β-γ space, and the nearly marginal mode structure is highly localized at the resonant surface. For comparison, the beta limit given by the Suydam criterion is calculated for each equilibrium in Fig. 3.8. Table 3.1 shows both the beta limit obtained from Suydam criterion (3.25) at the resonant surface of the $(2, 1)$ mode, $\beta_{\rm S}$, and the one shown in Fig. 3.8(b), $\beta_{\rm n}$. From Table 3.1, in cases of $\alpha \geq 8$, the non-resonant type $(2, 1)$ modes are unstable even when the central beta value is smaller than the Suydam limit. The beta limit in case of $\alpha = 4$ almost coincides with the Suydam limit since the radial mode structure is highly localized around the resonant surface.

α	$\beta_{\rm S}$	$\beta_{\rm n}$	p'
4	1.91×10^{-3}	2.07×10^{-3}	-0.707
8	1.53×10^{-2}	5.92×10^{-3}	-8.84×10^{-2}
10	4.90×10^{-2}	7.02×10^{-3}	-2.76×10^{-2}
14	0.560	8.39×10^{-3}	-2.41×10^{-3}

Table 3.1: Comparison between the marginal beta values from Suydam criterion, $\beta_{\rm S}$, and the ones shown in Fig. 3.8(b), $\beta_{\rm n}$. The equilibrium pressure gradient at the resonant surface is also shown. The pressure is normalized by the central value and the radial variable by the minor radius of the plasma column.

Finally, we considered a reversed shear profile, which will be realized in the high beta equilibrium of toroidal stellarator. Here we assume a cylindrical plasma with $\iota' < 0$ in the central region and $\iota' > 0$ in the outer region. We also assume the following profile of the rotational transform,

$$\iota = \iota(0) + \sigma r^2 - \lambda \exp\Big[-\frac{1}{2}\Big(\frac{r - r_{\rm c}}{W}\Big)^2\Big], \tag{3.34}$$

where σ is the previously defined shear parameter, $r_{\rm c}$ is the parameter for the minimum point of $\iota(r)$, and W denotes the characteristic width of non-monotonic region of $\iota(r)$. Here $\sigma = 0.2$, $r_{\rm c} = 0.5$, $W = 0.15$, and $\lambda = 0.2$ are chosen as an example. The pressure profile is again assumed to be parabolic, $p = p_0(1-r^2)$. We have calculated two cases which are parameterized as follows. One is the double resonant case, $\iota(0) = 0.6$, in which the radial positions of two resonant surfaces for the $(2, 1)$ mode are at 0.35 and 0.59, where the beta limits predicted from the Suydam criterion (3.25) are 6.61×10^{-3} and 8.25×10^{-3}, respectively. The other is the non-resonant case, $\iota(0) = 0.66$, in which the rotational transform has its minimum value 0.508 at $r = 0.478$. The both profiles of the rotational transform and the nearly marginal mode structures are shown in Fig. 3.9.

In the double resonant case the radial mode structure is localized dominantly at the inner resonant surface. The reason is that, since the beta limit from the Suydam criterion is lower at the inner resonant surface than that at the outer one, the pressure driven mode is more unstable at the inner resonant surface. In the non-resonant case the radial mode structure is restricted near the minimum point of the rotational transform and the beta limit is much lower than that in the double resonant case. It can be interpreted that, since the pressure driven mode is excited near the minimum point of ι in the non-resonant case, which is fairly close to $\iota = 0.5$, the stabilizing magnetic shear is very weak there. On the other hand, the resonant mode is localized at the resonant surface where the magnetic shear is relatively strong in the double resonant case, thus the beta limit becomes higher than that in

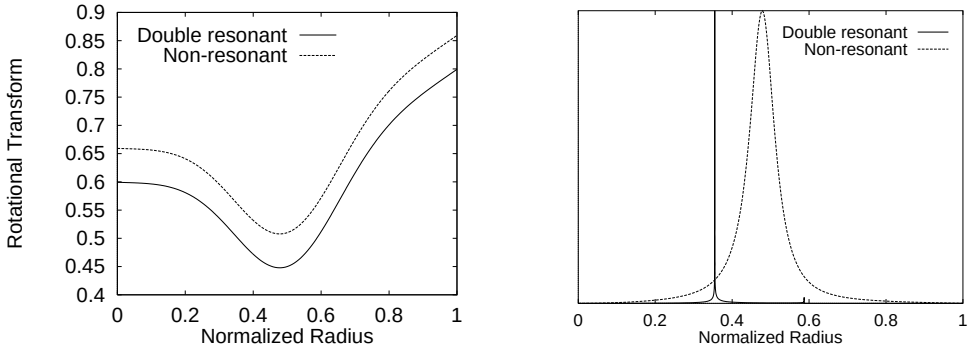

(a) (b)

Figure 3.9: (a) Profiles of the rotational transform for $\iota(0) = 0.6$, $\sigma = 0.2$, $r_c = 0.5$, $W = 0.15$, $\lambda = 0.2$ (double resonance) and $\iota(0) = 0.66$, $\sigma = 0.2$, $r_c = 0.5$, $W = 0.15$, $\lambda = 0.2$ (no resonance). (b) Radial mode structure of the $(2, 1)$ mode near the beta limit; $\beta_0 = 7.79 \times 10^{-3}$ for double resonant case, or $\beta_0 = 4.87 \times 10^{-4}$ for non-resonant case.

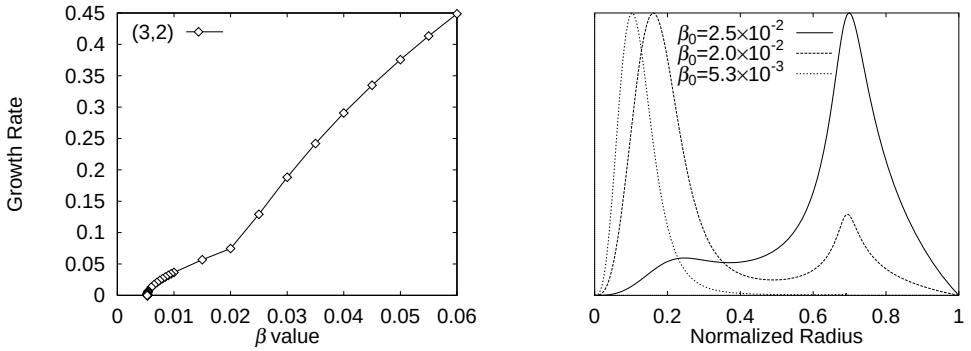

(a) (b)

Figure 3.10: (a) Growth rate as a function of β_0. (b) Radial mode structures for $\beta_0 = 2.5 \times 10^{-2}$, 2.0×10^{-2}, 5.3×10^{-3}. The beta limit is estimated as 5.27×10^{-3}, which is lower than the Suydam limit at the resonant surface of the $(3, 2)$ mode.

the non-resonant case.

We have also calculated the $(3, 2)$ mode in the non-resonant case with the rotational transform shown by dashed line in Fig. 3.9(a). This mode has one resonant surface at $r_s = 0.691$, where the beta limit from the Suydam criterion is $\beta_S = 8.28 \times 10^{-3}$. The numerical results are shown in Fig. 3.10. Figure 3.10(a) shows a transition in the growth rate depending on β_0, which occurs at $\beta_0 \sim 0.02$.

This transition is understood from the mode structures shown in Fig. 3.10(b). The maximum point of the unstable mode structure is placed at the resonant surface for $\beta_0 \gtrsim 0.025$. However, it moves to the inner weak shear region for the non-resonant type mode with $\beta_0 \lesssim 0.02$. This type of mode structure has a small peak at r_s near the beta limit, however, it does not decrease to zero at the resonant surface as shown previously, since the pressure gradient is not small there.

3.5 Summary

We have clarified the properties of the non-resonant pressure driven instabilities and the relation to the resonant instabilities in the cylindrical plasma model. The behavior of the non-resonant type mode depends strongly on the profile of both the pressure and rotational transform. For some cases the instability has a mixed character between the resonant and non-resonant modes. Also the transition from the resonant mode to the non-resonant type one occurs, when the pressure gradient is increased in the central region or the pressure profile becomes peaked.

At first we have solved the eigenmode equation analytically with respect to the perturbed stream function for an equilibrium with a constant rotational transform and a parabolic pressure profile. It is noted that the non-resonant mode has a global structure, and the dependency of γ on β is parabolic [see Eq. (3.18)]. In this case it can be shown that, the mode with fewest node number has the larger growth rate, and the higher harmonic mode with the same helicity has the higher beta limit.

With the numerical calculations, it is shown that the growth rate of the non-resonant mode decreases to zero without the tail near the beta limit, while the resonant mode has a fairly wide small growth rate regime expressed as $\gamma \propto e^{-1/\sqrt{\beta_0-\beta_S}}$ [126], where β_S denotes the central beta value given by the Suydam criterion. A physical interpretation is as follows. Although the resonant mode becomes localized at the resonant surface with the decrease of the beta value, the non-resonant mode does not have such a surface in the plasma column. Therefore the free energy necessary to excite the non-resonant modes is always finite, since the parallel wave number along the magnetic field line is also finite. Thus the growth rate decreases to zero without the tail near the beta limit. In the resonant case, since the higher harmonic modes have larger poloidal and toroidal wave numbers than the fundamental one, they can be more localized in the radial direction. Thus the growth rates at the same beta value are larger than the fundamental mode. However, all modes can be highly localized at the resonant surface as the central beta value decreases, the beta limit does not depend on the mode numbers and agrees with the Suydam limit. On the contrary, in the non-resonant case, since the parallel wave number

of higher harmonic mode becomes larger than the fundamental mode, the higher harmonics need more energy for excitation in the low beta regime. Thus the beta limit of the non-resonant mode with a higher harmonic mode number is larger than the fundamental mode.

When the pressure profile becomes locally flattened with the width of W around the resonant surface, the resonant mode shows the non-resonant feature. The beta limit in this case is increased with the small flattening region. The marginal mode structure is quite different from the case with $W = 0$, i.e. it is restricted to the one side of the resonant surface and the growth rate decreases to zero without the tail when β_0 approaches to the marginal value. It is noted that this non-resonant feature also appears in case of the nonzero but small pressure gradient at the resonant surface.

In Heliotron-E, when the beta value is increased, the central rotational transform is increased and the profile becomes non-monotonic. We have studied this situation by changing the rotational transform artificially. Even if there is no resonant surface for the $(2, 1)$ mode, when the minimum of the rotational transform, $\iota_{\min}$, is close to 0.5, the non-resonant $(2, 1)$ mode becomes unstable, which is independent of the Suydam criterion. When $\iota_{\min}$ is less than 0.5, the double resonant mode becomes unstable. Also, the non-resonant type $(3, 2)$ mode is unstable below the Suydam limit at the $\iota = 2/3$ surface. In this case the radial mode structure is observed in the central region when $\iota(0)$ is sufficiently close to $2/3$.

In later publications, the analytically approximated solution is obtained for cylindrical model equilibrium with the assumption that the mode structure has a step like structure around the resonant surface [46, 47]. It is shown that the beta limit of the non-resonant mode becomes mostly an order of magnitude higher than that obtained from Suydam criterion for the smooth pressure profile. Moreover, the toroidal effect on the non-resonant mode is also analyzed for the typical LHD configuration by means of the numerical computation [85, 87, 88]. The radial step like structure is also found in the toroidal case for the eigenmode with the toroidal mode number $n = 1$, however, it is not the case that the eigenmode with the least node number is the most unstable one.